

2 Material and Methods

2.1 Model systems

Model systems were chosen to mimic typical DEER application scenarios for which the relaxation behaviour of the nitroxide spin in the different spin environments (i.e. protonated, partly or completely deuterated solvent) was studied.

TEMPOL served as a model system to study the direct solvent influence on the relaxation behaviour of the nitroxide spin. For this system two different concentrations ($\approx 10 \mu\text{M}$ and $100 \mu\text{M}$) which lie within the typical DEER concentration range were used to examine the effect of sample concentration on relaxation.

The double mutant T4 Lysozyme-72-131 represents the class of soluble proteins with a spin environment consisting of solvent as well as protein.

WALP23 is a synthesised α -helical trans-membrane peptide which was chosen as a model for proteins in a lipid membrane.

The rigid biradial MSA236 served as a sample with a well defined distance due to minimised conformational flexibility which allowed for DEER calibration measurements. Its chemical structure is shown in Fig. 15b on page 55. The relaxation behaviour of this system was approximated by a structurally similar rigid monoradical MS 107 as shown in Fig. 4. Relaxation traces measured on the biradical would otherwise display dipolar modulation which would complicate the extraction of the relaxation law.

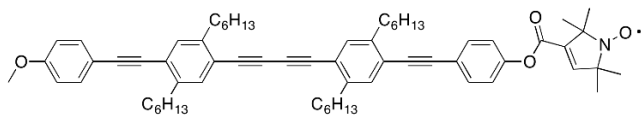


Fig. 4: Chemical structure of monoradical MS 107 with close structural resemblance to the biradical MSA 236. This allows to mimic the relaxation behaviour of the biradical.

- TEMPOL in
 - H₂O-Glycerol (HGly)
 - H₂O-deuterated Glycerol (d₈Gly)
 - D₂O-d₈Gly
- T4 Lysozyme-72-131 in
 - H₂O-HGly
 - H₂O-d₈Gly
- WALP23-2 in
 - H₂O
 - D₂O
- WALP23-11 in
 - H₂O
 - H₂O-d₈Gly
- Rigid Monoradical MS 107 in deuterated *o*-terphenyl (d₈-OTP)
- Rigid Biradical MSA 236 in d₈-OTP

2.1.1 Sample preparation

1:1 volume mixtures of HGly or d₈Gly and H₂O or D₂O were used to avoid crystallisation upon freezing TEMPOL or T4 Lysozyme samples in liquid nitrogen.

2.1.1.1 TEMPOL

10 μM and 100 μM TEMPOL solutions were prepared from a 1 mM TEMPOL stock solution in DMSO by diluting to 20 μM and 200 μM with H_2O or D_2O and addition of HGly or d_8Gly . The exact spin concentration was measured using continuous wave (CW) EPR relative to a reference sample of known spin concentration.

2.1.1.2 Rigid radicals MS 107 and MSA 236

The synthesis of the monoradical MS 107 and biradical MSA 236 was carried out by Professor A. Godt at Bielefeld University, Germany. A solid 50 μM mixture of either sample with $\text{d}_8\text{-OTP}$ was placed into a sample tube and melted with a heat gun at 70 $^\circ\text{C}$, a glassy frozen sample was obtained by subsequent shock-freezing in liquid nitrogen.

2.1.1.3 T4 Lysozyme

A T4 Lysozyme double mutant with cysteine residues included at sites 72C and 131C was spin labelled with (1-Oxyl-2,2,5,5-tetramethylpyrroline-3-methyl) methanethiosulfonate (MTSSL). The spin labelling protocol involved breaking of the S-S bridges via reduction using 20 μL of a freshly prepared 100 mM butan-2,3-diol-1,4-dithiol (DTT) solution for 2 mL cooled protein. The sample was incubated for two hours at 4 $^\circ\text{C}$. Subsequently, DTT was removed with a PD_{10} column using a gravity protocol and buffer pH set to 7.6 (40 mM NaCl, 25 mM 3-morpholinopropane-1-sulfonic acid (MOPS), 10 % H-Gly). For the labelling step two-fold label concentration per site relative to the protein concentration was used. The MTSSL solution was added immediately to the eluate from the column and was incubated for another 30 minutes while agitated at room temperature. The remaining free label was removed by a PD_{10} column and 10 kDa centricons were used for concentrating the sample. The final protein concentration was obtained from UV absorbance at 280 nm whereas the spin concentration was measured by CW EPR relative

to a standard TEMPOL sample of known concentration. The final sample was obtained by adding HGly or d₈Gly in equal amounts to the spin labelled Lysozyme resulting in a final spin concentration of $\approx 13 \mu\text{M}$. The modulation depth of 0.454 in a 4-DEER trace acquired with the commercial Q-band spectrometer as described in section 2.2.2.2 indicates a labelling efficiency of $> 95\%$.

2.1.1.4 WALP23

The single mutants WALP23-2 and WALP23-11 of nominal $50 \mu\text{M}$ were spin labelled using MTSSL as part of a semester project by Max Doppelbauer. Details on the spin labelling procedure and probe preparation are specified in^[24] under 3.1 '*Sample Preparation*'.

2.2 Instrumentation

2.2.1 X band

For CW EPR measurements of the spin concentration of TEMPOL and T4 Lysozyme samples a Bruker E500 X-band spectrometer operated by Xepr 2.2b.27 on a Suse 8.2 Linux with a Bruker SHQ resonator was used.

All pulsed experiments at X-band frequencies were performed on a home-built X-band spectrometer in combination with an arbitrary waveform generator (AWG) further specified in^[25] under 2.1 '*Instrumentation*'.

2.2.2 Q band

2.2.2.1 Home-built spectrometer

Relaxation measurements for all TEMPOL samples were carried out using the home-built Q-band spectrometer operated from a standard console (Bruker) and equipped

with a pulsed traveling wave tube (TWT) amplifier. The output power amounts to 150 W. The home-built TE102 rectangular resonator allowed for usage of oversized tubes of 3.0 mm diameter.^[15]

2.2.2.2 Commercial

All Q-band DEER experiments as well as relaxation measurements (apart from TEMPOL samples) were performed on a commercial Bruker Elexsys E580 Q-band spectrometer with an output power of 200 W. Shaped pump pulses were generated with an Agilent M8190A 12 GS/s AWG. A more detailed description of the instrumentation can be found in^[26] under 3.2 '*Instrumentation*'.

2.3 Experiments

All pulsed EPR measurements were performed at 50 K with $\approx 40 \mu\text{l}$ sample volume in quartz tubes of $\approx 3.0 \text{ mm}$ outer diameter. The integration gate at the acquisition position was centered around the echo maximum whereas the width was set to twice the observer pulse length (24 ns). For offset-free signal detection a $[(+x) - (-x)]$ phase cycle on every initial $\pi/2$ pulse of the pulse sequences was carried out.

For concentration measurements using CW EPR $2 \mu\text{l}$ sample volume was filled in glass capillaries.

2.4 Relaxation Measurements

Relaxation measurements with the observer sequence of the corresponding 4-, 5-, 7- and 9-DEER (corresponding to order $n = 1, 2, 3$ and 4) and 7 and 9-Uhrig-DEER ($n = 3$ and 4) experiments were performed on TEMPOL, T4 Lysozyme, WALP23 and the monoradical MS 107 under the above specified conditions at Q band.

For MSA 236 and T4 Lysozyme, relaxation experiments were also carried out at X band

prior to corresponding DEER experiments for 4-, 5- and 9-DEER scheme as well as the 9-Uhlig scheme. Where the setup in terms of delays and pulse duration corresponds to the respective DEER observer sequence as described below.

2.4.1 Pulse sequences

Fig. 5 displays the pulse sequences employed for the relaxation measurements with pulse lengths $t_{\pi/2} = t_{\pi} = 32$ ns at X band and $t_{\pi/2} = t_{\pi} = 12$ ns at Q band. All time delays after generation of the primary echo ($\pi/2 - \tau/n - \pi$) were incremented by $\Delta t = 4$ ns, shifting the acquisition position accordingly. All relaxation traces displayed in this thesis such as in Fig. 11 have an x -axis corresponding to the absolute time. To allow for comparison of the echo intensity as a function of time the initial acquisition time for $\Delta t = 0$ was chosen identical for all relaxation pulse sequences.

The 4-DEER and 5-DEER relaxation sequence share the same number of pulses whereas the latter is characterised by symmetric pulse delays ($\tau/2 - \tau - \tau/2$) as can be seen in Fig. 5. Due to imperfect pulses a stimulated echo ($\pi/2 - \tau/2 - \pi/2 - \tau/2 - \pi/2$) additionally to the desired refocused echo ($\pi/2 - \tau/2 - \pi - \tau/2 - \pi$) arises at the 5-DEER-acquisition position. This complication does not occur in the 4-DEER setup as depicted in Fig. 6. To measure the relaxation of the pure refocused echo the stimulated and refocused echo needed to be separated in time by shifting the second π pulse by the delay $\delta\tau$ as illustrated in Fig. 6b. Delay $\delta\tau$ was chosen such that it only corresponds to a fraction of the total sequence time. This allows to neglect any relaxation occurring during the additional $\delta\tau$ time. Setting $\delta\tau = 0$ in a relaxation measurements leads to an underestimation of the real relaxation time as the stimulated echo signal contribution decays with approximately T_1 .

Instead of the introduced time shift, stimulated and refocused echo could be alternatively separated by phase cycling. Whereas this approach is feasible for the 5-DEER sequence, the number of required cycles quickly increases with additional π pulses. More specifically two π refocusing pulses require a four-step phase cycle, such that

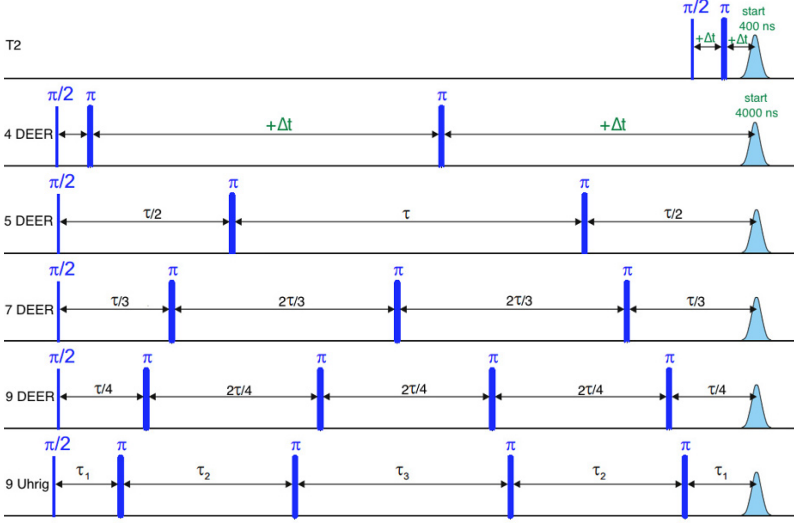
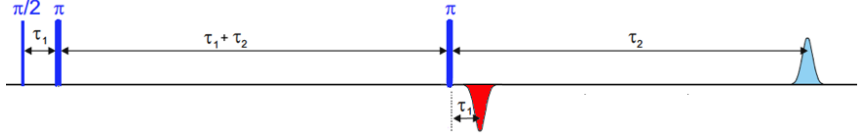


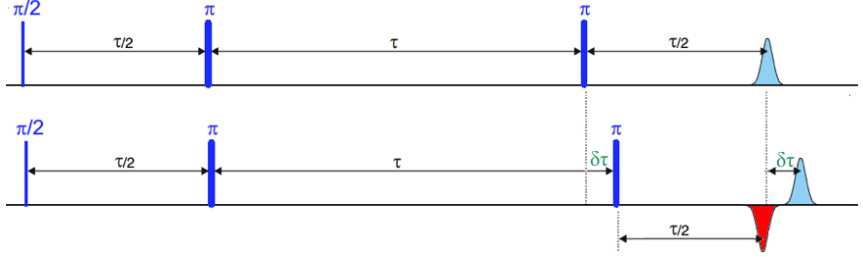
Fig. 5: Pulse sequences for T_2 relaxation measurements including the standard primary echo setup as well as DEER observer frequency derived sequences. The basis τ for the 4, 5, 7- and 9 DEER sequences were chosen so that the initial distance between the first pulse in the sequence and the echo is identical in all measurements. The time delays τ_1 , τ_2 and τ_3 for the 7 and 9-Uhrig sequence were obtained from equation (35) for $T = t_{\text{acq}}$. 7-Uhrig is not displayed here.

for a number m of π refocusing pulses in the observer sequence a 2^m step phase cycle is required. This significantly increases the number of necessary acquisitions per experiment.

Therefore a time separation represents the more elegant approach and was used for all DEER sequences of order $n = 1, 2, 3$ and 4 and Uhrig-DEER sequences of order $n = 3$ and 4. Increasing the number of π pulses does not only lead to different stimulated echos but additionally creates a number of refocused echos. For the 7-DEER sequence already four different echos were observed at the proximity of the acquisition position and care had to be taken to select the correct echo for signal acquisition. For the DEER relaxation measurements crossing echos for all sequences of order $n > 2$ were observed,



(a) 4-DEER observer sequence with stimulated echo (dark) at $3\tau_1 + \tau_2$ naturally separated in time from the refocused echo (light) at $2\tau_1 + 2\tau_2$ of opposite phase.



(b) 5-DEER observer sequence overlap of stimulated (dark) and refocused echo (light) with opposite phase at the acquisition position. Upon shifting the last π pulse by delay $\delta\tau$ the two echos are separated in time.

Fig. 6: Stimulated and refocused echo positions in 4- and 5 DEER observer scheme.

such that a negative time shift $\delta\tau$ was employed to all π pulses after the primary echo part of these sequences.

2.5 DEER Measurements

2.5.1 Pulse sequence

The 5-DEER scheme introduced by Borbat, Georgieva and Freed is displayed in Fig. 3c and shows the figure from the original publication.^[4] This sequence is recovered upon adding a pump pulse sequence at ω_B to the stationary $(\pi/2 - \tau/2 - \pi - \tau - \pi - \tau/2)$ sequence as displayed in Fig. 6b ($\delta\tau = 0$).

In section 2.4.1 complications arising from overlapping stimulated and refocused echo for relaxation measurements have been discussed. Fig. 7 illustrates the effect for DEER measurements as the unshifted 5-DEER scheme leads to a reduction in modulation

depth Δ . This effect is due to the unmodulated stimulated echo signal contribution at the acquisition time. Note that the 5-DEER publication by Borbat, Georgieva and Freed does not discuss this issue.^[4]

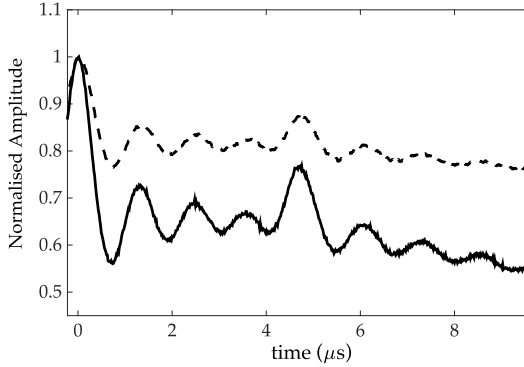
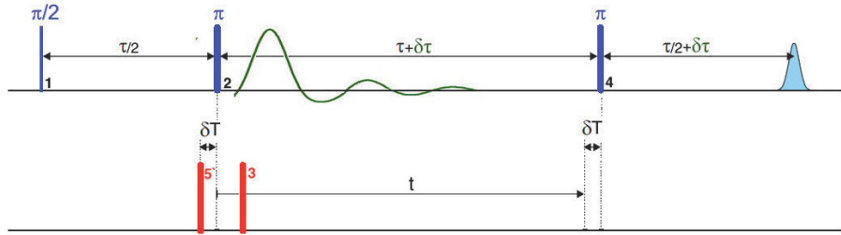


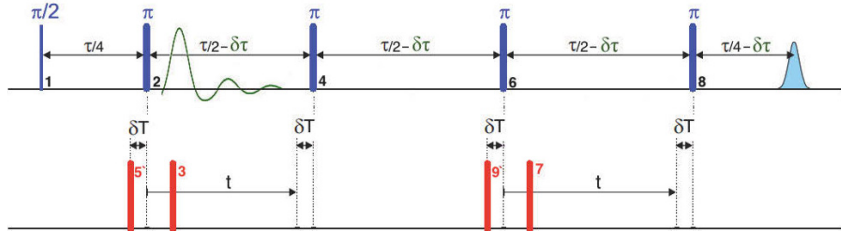
Fig. 7: Rect-5'-DEER traces for MSA 236 at Q band obtained with the 5'-DEER sequence as shown in Fig. 6b with setting $\delta\tau = 0$ ns (---) where stimulated and refocused echo overlap at the acquisition position. With $\delta\tau = 72$ ns (—) the unmodulated stimulated echo does not contribute to the signal at the acquisition position any longer. A significant increase in modulation depth Δ is visible.

Implementation of the original 5-DEER scheme was not possible due to restrictions in the Bruker PulseSpel Software which generally does not allow negative time increments. In other words, pushing the pump pulse 3 from right to left as shown in Fig. 3c could not be realised. Hence, the sequence was adjusted to a 5'-DEER scheme such that the time delay t was incremented and the stationary pump pulse was moved to position 5' as depicted in Fig. 8a. The dashed sequence nomenclature refers in the following to DEER experiments with pump pulses at the just specified position. In contrast, the dashed nomenclature does not apply to the standard 4-DEER experiment nor to higher order relaxation setups. Additionally to the 5' pump pulse, the second observer π pulse was shifted to obtain a pure refocused echo at $(2\tau + 2\delta\tau)$. The dipolar evolution time for the modified 5'-DEER scheme can be obtained as described in section 1.4.3.1 and amounts to $t_{\text{dip}}^{5'\text{-DEER}} = 2(t - \delta T)$ such that the signal is modulated with $\cos[d(t - \delta T)]$

which is identical to the 5-DEER signal modulation defined in equation (30). The time origin of the dipolar evolution occurs for $t = \delta T$ in both 5-pulse schemes, however the 5' setup reaches this point earlier in time. This is experimentally more convenient and results in a reversal of the modulated time trace relative to the Borbat, Georgieva and Freed 5-DEER setup. To obtain a deadtime-free 5'-DEER sequence, δT has to be chosen larger than the minimum delay t_{\min} between a pump and an observer pulse. This experimental condition applies to all higher order CP derived DEER sequences.



(a) 5'-DEER scheme with reversed modulated time trace relative to 5-DEER as shown in Fig. 3c.



(b) Extension of 5'-DEER to a 9'-DEER experiment which corresponds to $N = 2$ for the scheme displayed in Fig. 3c with adjustments analog to the 5'-DEER sequence. As indicated the dipolar time decreases whereas the signal oscillates with doubled frequency with respect to the 5'-DEER signal if the same pump pulse increment is applied to both pulses 3 and 7.

Fig. 8: 5'-DEER and 9'-DEER experiments with fixed interpulse delays in the observer sequence (with pulses 1, 2, 4 etc.) at ω_A which also applies to the delay δT in the pump sequence (with pulses 5', 3 etc.) at ω_B . The relative position of pump pulse 3 (and 7) is moved by incrementing t . A deadtime-free sequence is obtained for $\delta T > t_{\min}$ with t_{\min} being the minimum delay between a pump and an observer pulse to prevent pulse overlap artifacts. The numbering of the pulses follows the original scheme as displayed in Fig. 3a.

DEER experiments of even order n were carried out which are analogue to the DEER relaxation setups and require addition of an even number n pump pulses. This is an advantage in case of adiabatic chirp pump pulses as recognised by Spindler.^[5] The frequency sweep, characteristic for the chirp pulse, leads to a dispersion in terms of pump spin inversion times. For an even number of chirp pulses this dispersion can be refocused by applying chirp pairs with opposite sweep direction. Because this refocusing is incomplete for an odd number of pump pulses the 7-DEER scheme was not considered.

Therefore 9-DEER corresponds to the next higher order of dynamical decoupling and is characterised by $n = 4$. This experiment can be obtained by simply repeating the 5-DEER scheme as already suggested by Borbat, Georgieva and Freed.^[4] The symmetrised 9-DEER scheme suffers from the same stimulated echo complications as the 5-DEER setup, so that the $n = 4$ DEER experiment was implemented as 9'-DEER experiment shown in Fig. 8b. The observer spin echo refocuses at $(2\tau - 4\delta\tau)$ with $t_{\text{dip}}^{9\text{'-DEER}} = 4(t - \delta T)$, such that the amplitude is modulated by $\cos[2d(t - \delta T)]$. The upper bound of both variable pump pulse delays is $t \leq \tau/2 - \delta\tau - \delta T$, leading to a maximum dipolar evolution time of $t_{\text{dip, max}}^{9\text{'-DEER}} = 2\tau - 4\delta\tau - 8\delta T$ relative to $t_{\text{dip, max}}^{5\text{'-DEER}} = 2\tau + 4\delta\tau - 2\delta T$. Due to the opposing sign of $\delta\tau$ for the 5'-DEER and 9'-DEER setup, the available dipolar evolution time $t_{\text{dip, max}}^{5\text{'-DEER}}$ appears to be longer than $t_{\text{dip, max}}^{9\text{'-DEER}}$ for the same choice of τ , $\delta\tau$ and δT . However, as $\delta\tau$ and δT are set to much shorter lengths relative to τ , the gain in maximum dipolar evolution time for the 5'-DEER sequence is only small. However the 9'-DEER scheme has an advantage for big enough ξ values such that the refocusing allows to choose longer τ values for the 9'-DEER experiment relative to the 5'-DEER setup.

In analogy to equation (30) on page 18 the intramolecular echo amplitude modulation function for the 9'-DEER setup $V^{9\text{'-DEER}}(t)$ can be derived. This expression is made up of 2^4 terms. However as only the contributions that depend on t are relevant for the 9'-DEER trace, signal contributions arising from $(q_3p_5'p_7p_9')$, $(p_3q_5'p_7q_9')$, $(q_3p_5'q_7p_9')$, $(q_3p_5'q_7q_9')$ and $(q_3q_5'q_7q_9')$ are not listed. The angular brackets denote again

the average over all p_k, q_k and interspin vector orientations hidden in d .

$$\begin{aligned}
V^{9'\text{-DEER}}(t) \propto & \langle (p_3 p_5' p_7 p_{9'}) \cos [2d(t - \delta T)] + (p_3 q_5' p_7 p_{9'}) \cos [2d(t - \delta T/2 - \tau/8)] \\
& + (q_3 p_5' p_7 p_{9'}) \cos [d(t - \tau/4)] + (p_3 p_5' q_7 p_{9'}) \cos [d(t - 2\delta T + \tau/4)] \\
& + (p_3 q_5' q_7 p_{9'}) \cos [d(t + \delta\tau - \delta T)] + (q_3 p_5' p_7 q_{9'}) \cos [d(t - \delta\tau - \delta T)] \\
& + (q_3 q_5' p_7 p_{9'} + p_3 p_5' q_7 q_{9'}) \cos [d(t - \delta T)] + (q_3 q_5' p_7 q_{9'} + p_3 q_5' q_7 q_{9'}) \cos [d(t - \tau/4)] \rangle
\end{aligned} \tag{36}$$

Expression (36) can be simplified by two assumptions: First, equal spin inversion probabilities for each pump pulse (3, 5', 7 and 9') are assumed. This assumption is reasonable if pump pulses are well reproducible once the respective pulse parameters have been set. Secondly as $p \ll q$ holds for optimised pump pulses, terms of low probability in equation (36) can be neglected, leading to

$$\begin{aligned}
V^{9'\text{-DEER}}(t) \propto & \langle p^4 \cos [2d(t - \delta T)] + p^3(1 - p) \cos [2d(t - \delta T/2 - \tau/8)] \\
& + p^3(1 - p) \cos [d(t - \tau/4)] + p^3(1 - p) \cos [d(t - 2\delta T + \tau/4)] \rangle
\end{aligned} \tag{37}$$

where the relation $q = (1 - p)$ was used. Here the angular brackets denote the average over all interspin vector orientations hidden in d . As $\frac{p^4}{p^3(1-p)} = \frac{p}{(1-p)}$ applies, the signal contributions weighted by $p^3(1 - p)$ in equation (37) are expected to scale comparable to the symmetric 4-DEER artifact in the 5-DEER signal for identical pump pulses. Therefore, additionally to the main 9'-DEER signal contribution three additional terms have to be considered corresponding to $(p_3 q_5' p_7 p_{9'})$, $(p_3 p_5' p_7 q_{9'})$ and $(p_3 p_5' q_7 p_{9'})$. In expression (37) the first $p^3(1 - p)$ term refocuses at $t = \delta T/2 + \tau/8$. As $\tau \gg \delta T$ the two signal contributions are well separated in time. The third and fourth term in equation (37) are only modulated with half the dipolar frequencies as either one of the moving pump pulses enter with q into the expression. For the above specified experimental conditions both terms refocus at similar dipolar time t . Hence the $(q_3 p_5' p_7 p_{9'})$ and $(p_3 p_5' q_7 p_{9'})$ terms coincide in time and can be viewed as the analogue to the $p_3 q_5$ signal contribution in the 5'-DEER setup.

In modification of the CP inspired multipulse DEER setups the observer sequence may

also be modified to a Uhrig decoupling scheme. For order $n = 2$ this coincides with the symmetric CP pulse arrangement as used in 5-DEER. A possible 7-Uhrig-DEER sequence was not considered due to the uneven number of pump pulses. Therefore a 9'-Uhrig-DEER experiment as depicted in Fig. 9 allows for the implementation of this asymmetric DD observer scheme.

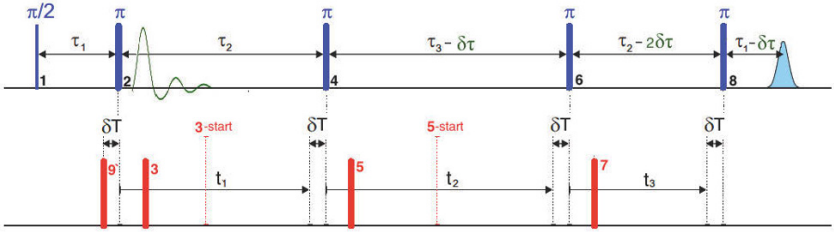


Fig. 9: 9'-Uhrig-DEER sequence with interpulse delays τ_1 , τ_2 and τ_3 defined by equation (35) on page 24 for a total sequence length of T . Relative to the 9'-DEER setup the position of the first π pump pulse 9' is kept fixed at a delay δT whereas pump pulses 3, 5 and 7 are pushed with identical increments ($t = t_1 = t_2 = t_3$) so that the smallest interpulse delay between observer pulses 6 and 8 determines the available dipolar evolution time. For t increments identical in size to the 5 pulse scheme, the signal oscillates with three times the frequency with respect to 5'-DEER modulation for identical incrementation of t . The time shift $\delta\tau$ reduces the available time window, yet allows for a stimulated-echo-free acquisition position. Setting $t_{3, \min}$ and $t_{5, \min}$ to the dashed starting position labelled 3- and 5-start, allows to reduce t_{\min} .

Similar to the derivation of equation (37) for the 9'-DEER sequence, only signal contribution with weight p^4 and $p^3(1 - p)$ are discussed in the following for the 9'-Uhrig sequence. The expression for the 9'-Uhrig intramolecular echo amplitude modulation function $V^{9'\text{Uhrig}}(t)$, specified in equation (38), is independent of the interpulse delay τ_3 . This delay can be eliminated by the refocusing condition $\tau_3 = 2(\tau_2 - \tau_1)$.

$$\begin{aligned}
V^{9'-\text{Uhrig}}(t) \propto & \langle (p_3 p_5' p_7 p_{9'}) \cos [d (2\tau_1 - 2\tau_2 + \delta T + \delta\tau + (t_1 + t_2 + t_3))] \\
& + (p_3 p_5' p_7 q_{9'}) \cos [d (2\tau_2 - \tau_1 - \delta\tau - (t_1 + t_2 + t_3))] \\
& + (q_3 p_5' p_7 p_{9'}) \cos [d (2\tau_2 - \tau_1 - \delta T - \delta\tau - (t_2 + t_3))] \\
& + (p_3 q_5' p_7 p_{9'}) \cos [d (\tau_2 - \tau_1 - \delta T - \delta\tau + (t_1 - t_3))] \\
& + (p_3 p_5' q_7 p_{9'}) \cos [d (\tau_1 - \tau_2 - \delta T + t_3)] \rangle
\end{aligned} \tag{38}$$

The convenient choice of $t = t_1 = t_2 = t_3$, uses the same time increment t for all pump pulses 3, 5 and 7. Applying the same assumptions as used for simplifying equation (36) to (37), leads to

$$\begin{aligned}
V^{9'-\text{Uhrig}}(t) \propto & \langle p^4 \cos [d (2\tau_1 - 2\tau_2 + \delta T + \delta\tau + 3t)] + p^3(1-p) \cos [d (2\tau_2 - \tau_1 - \delta\tau - 3t)] \\
& + p^3(1-p) \cos [d (2\tau_2 - \tau_1 - \delta T - \delta\tau - 2t)] + p^3(1-p) \cos [d (\tau_1 - \tau_2 - \delta T + t)] \rangle
\end{aligned} \tag{39}$$

Note, how the fourth signal contribution in equation (38) ($p_3 q_5' p_7 p_{9'}$) vanishes for $t_1 = t_3$. Considering the main signal modulation with weight p^4 , the minimum dipolar evolution time is reached at $t_{1,\min} = t_{2,\min} = t_{3,\min} = \delta T$ and corresponds to $t_{\text{dip},\min}^{9'-\text{Uhrig}} = 2\tau_1 - 2\tau_2 + 4\delta T + \delta\tau$. For $t_{\text{dip},\min}^{9'-\text{Uhrig}} < 0$ the time origin is sampled, a condition which is fulfilled for the 9'-Uhrig setup due to two reason. First of all, δT and $\delta\tau$ are both chosen to be much shorter than any Uhrig interpulse delay τ_j . Secondly, $\tau_2 > \tau_1$ holds according to equation (35) on page 24. The smallest interpulse delay between the observer pulses 6 and 8 determines the the maximal time window over which t can be incremented, as illustrated in Fig. 9. Instead of starting with $t_{1,\min} = t_{2,\min} = t_{3,\min} = \delta T$, the initial delays $t_{1,0}$ and $t_{2,0}$ can be set to $t_{1,0} = \delta T + \delta\tau$ and $t_{2,0} = \delta T + \delta\tau + (\tau_3 - \tau_2)$. Using again the refocusing condition, this setup yields $t_{\text{dip},\min}^{9'-\text{Uhrig}} = 6\delta T + \delta\tau - \tau_2$ and corresponds to starting position of pump pulses 3 and 5 indicated by the dashed lines labelled 3- and 5-start respectively in Fig. 9. This allows to reduce the fraction of dipolar evolution observed before the time origin as $|t_{\text{dip},\min}^{9'-\text{Uhrig}}| < |t_{\text{dip},\min}^{9'-\text{Uhrig}}|$ applies.

Moreover equation (39) shows three additional signal contribution, each weighted by

$p^3(1 - p)$. The $(p_3p_5'p_7q_9')$ contribution is modulated with the same frequency as the desired p^4 weighted signal, but is separated in time by $\tau_1 + \delta T$. Signal artifacts arising from $(q_3p_5'p_7p_9')$ and $(p_3p_5'q_7p_9')$ can also be distinguished from the main signal as they are only modulated by two thirds or a third of the main dipolar frequency.

Performing DEER experiments on a pair of nitroxide labels as observer and pump spin requires the excitation of two distinct regions of their nearly identical absorption spectrum. The nitroxide absorption spectrum differs for X- and Q-band frequencies, 9.5 GHz and 34.5 GHz respectively. This implies different pulse lengths and frequency offsets between pump and observer frequencies for artifact free DEER traces of optimal sensitivity.^[15] The DEER setup at the two frequencies is specified in the following.

2.5.1.1 X band

For X-band frequencies a 12-65-32 excitation scheme was used which applies pump pulses of 12 ns length on the central maximum of the spectrum. The observer frequency was placed at lower fields with a frequency offset of 65 MHz relative to the pump frequency. The observer pulses were adjusted to 32 ns for both $\pi/2$ and π pulses.^[15]

2.5.1.2 Q band

The nitroxide absorption spectrum at Q band is broader and more asymmetric with respect to X band. This allows for harder observer pulses of 12 ns lengths while choosing a bigger frequency offset of 100 MHz between the pump and the observer frequencies. Pump pulses were set to 12 ns as well, leading to a 12-100-12 excitation scheme.^[15] All pulses were adjusted by nutation experiments.

2.5.2 Pump pulses

Non-rectangular pump pulses were used to minimise the signal contribution from inverting pump spins once, but less than two or four times for 5'-DEER and 9'-DEER experiments, respectively. For the latter two experiments pump pulses were organised in pairs such that the frequency sweep was carried out in opposite directions in order to refocus pump spin inversion dispersion. Shaped adiabatic pump pulses were first tested on the model system MSA 236 and subsequently applied to T4 Lysozyme in H₂O-HGly.

2.5.2.1 Design

The optimised non-rectangular pump pulses were pre-simulated by a graphical user interface (GUI) programmed in Matlab by Andreas Dounas.^[11]

The programme allows to incorporate the resonator profile which was determined experimentally as described in subsection 2.5.3. This allowed to generate resonator compensated pump pulses which have been shown to enhance inversion performance.^[27] The convolution of the experimental resonator profile with the amplitude and frequency modulation function of the simulated pump pulse in the frequency domain gave a visual impression on the expected inversion quality. Furthermore, the GUI output nominal values for adiabaticity Q_{\min} and inversion I , as defined by equation (20) and (25), were used to find optimal pump inversion pulses for each experimental setup. Each pulse is defined by the central frequency, the sweep bandwidth $\Delta\nu$ both in GHz and the pulse length t_p in ns. HSh pulses required as specification the order h and the parameter β_{HS} . For asymmetric HSh pulses h_l and h_r defined the left and right order for the respective pulse flank. Generally, optimal inversion performance can be achieved by steep edges and a flat pulse plateau in the frequency domain.

2.5.3 Resonator compensation

The direct relation between the nutation frequency of a resonant spin and the magnetic field strength for a given frequency f can be used to obtain the resonator profile $\nu_1(f)$ based on nutation experiments as described in section 1.4.2. Pulse lengths for X- and Q-band resonator profile characterisation were set to 16 ns ($\pi/2$) - 32 ns (π) and 12 ns ($\pi/2$) - 24 ns (π).^[27]

At Q band an RLC-resonator profile was fitted to the experimental profile to obtain parameters for resonator compensation incorporated into the pump pulse design. At X band, experimental $\nu_1(f)$ profiles were used for the pulse compensation.

Secondly, a non-linear calibration $\nu_1(a_s)$ of the digital pulse amplitude a_s was carried out as described in^[27] to compensate for amplitude imperfections introduced by the resonator profile and the deviation created in the TWT relative to the digital pulse.

2.5.3.1 Inversion characterisation

The inversion efficiency I as defined in equation (25) was used to characterise the pump pulses of various pulse shapes as a function of frequency (rectangular, linear chirp and HSh pulses). For this a Hahn echo scheme was used which is displayed in Fig. 1a.^[27] At Q band the pulse lengths were set to 12/24 ns whereas X-Band requires pulse lengths of 16/32 ns. The echo was integrated over 24 and 32 ns, respectively, by setting the observation frequency to the intended pump frequency in the DEER experiment. At X band, the excitation profile of a pulse was obtained by simultaneously stepping the observation frequency with the field. For monochromatic pump pulses, ν_1 corresponded to the observation frequency. For the linear chirp and HSh pulses the center frequency was stepped. At Q band only the observation frequency was incremented.

A phase cycle $[+(+x) - (-x)]$ on the first $\pi/2$ pulse allowed for offset cancellation.

2.5.4 *DEER signal analysis*

For standard DEER signal analysis DeerAnalysis^[28] was used. The procedure is summarised in section 1.4.4.

Dynamical Decoupling in Distance Measurements by
Double Electron-Electron Resonance

Soetbeer, J.M.

2016, XXI, 74 p. 24 illus., Softcover

ISBN: 978-3-658-14669-6